

Cite this article as: Wang Sufang, Wang Chengyue, Chen Liyong, et al. First-Principles Study of Half-Metallicity of Fe Nanobelts[J]. Rare Metal Materials and Engineering, 2021, 50(11): 3942-3948.

ARTICLE

First-Principles Study of Half-Metallicity of Fe Nanobelts

Wang Sufang¹, Wang Chengyue¹, Chen Liyong¹, Xie You¹, Zhang Jianmin²

¹ College of Science, Xi'an University of Science and Technology, Xi'an 710054, China; ² School of Physics and Information Technology, Shaanxi Normal University, Xi'an 710062, China

Abstract: The relaxed structures and electromagnetism properties of Fe nanobelts with different cross-sections of 3×5 , 3×7 , 3×9 , 3×11 , 3×13 , and 3×15 atom layers were investigated using the first-principles of projector-augmented wave (PAW) pseudo potential based on the density functional theory (DFT) framework. Results show that for all the Fe nanobelts, the relaxed structures retain the two-fold symmetry. However, the cross-section changes from rectangle shape in the beginning into a near-single-ellipse shape for the ones with atom layers of 3×5 and 3×7 , and into a double-ellipse shape for other atom layers with broader cross-sections. In addition, it is found that the Fe nanobelt with 3×7 atom layer is a half-metal material: electrons with either majority spin or minority spin can pass through the Fermi level. Therefore, it can be used in the field of spintronics for producing nearly 100% spin-polarized currents.

Key words: Fe nanobelt; relaxation; electronic structure; electromagnetism; density functional theory

As a new member of one-dimensional (1D) nanostructures, nanobelts with a rectangular cross-section, well-defined geometry, and a perfect crystalline form have attracted much attention because of their excellent catalyst performances and great potential in various fields such as electronics, optics, photonic technology, piezoelectricity, and especially nanodevices^[1-8]. Currently, the scanning tunneling microscopy (STM), atomic force microscopy (AFM), and high resolution transmission electron microscopy (HRTEM) are used to study the properties of nanobelts. Nanobelts have been synthesized using semiconductors, metals, and other materials.

Ultrathin magnetic nanobelts have great potential in applications of biomedicine, magnetic recording, and spintronic applications^[9-14]. Iron is a relatively abundant element and shows significant influence on the development of materials science. Pure Fe may be crystallized in several different structures, but the most common structure is the α -phase body-centered cubic (bcc) structure. Arrays of Fe bilayer nanobelts with perpendicular magnetization on a W(110) substrate can be observed by spin-polarized scanning tunneling spectroscopy (SPSTS)^[15-26]. Small domain structures may exist in long narrow ultrathin magnetic nanobelts with sufficiently large magnetic anisotropy^[17], which is essential for

applications in information science^[13,14]. It is highly desirable to investigate the effects of size on the relaxed structure and electromagnetic properties of ultrathin magnetic Fe nanobelts.

In this research, under generalized gradient approximation (GGA), calculations were performed to investigate the electromagnetic properties of Fe nanobelts with different cross-sections of 3×5 , 3×7 , 3×9 , 3×11 , 3×13 , and 3×15 atom layers using first-principles projector-augmented wave (PAW) pseudo potential based on density functional theory (DFT). The calculation method and model of Fe nanobelts of 3×5 atom layer were established and the electromagnetic properties of Fe nanobelts were analyzed.

1 Calculation Model and Method

In a top-down fabrication process, a rectangle nanobelt is usually cleaved from bulk crystals. Fig.1 shows the schematic diagram of a bcc Fe nanobelt with the cross-section of 3×5 atom layer. Assuming that the nanobelt along [001] direction has two (100) and two (010) lateral surfaces and an infinite length for avoiding end effects, wider nanobelts with cross-sections of 3×7 , 3×9 , 3×11 , 3×13 , and 3×15 atom layers can be obtained by maintaining the original three atomic layers along [100] direction and successively adding two atomic

Received date: April 12, 2021

Foundation item: National Natural Science Foundation of China (11447139, 11647051); Natural Science Basis Research Plan in Shaanxi Province of China (2015JQ1027); Scientific Research Program Funded by Shaanxi Provincial Education Department (14JK1482)

Corresponding author: Chen Liyong, Ph. D., Lecturer, College of Science, Xi'an University of Science and Technology, Xi'an 710054, P. R. China, Tel: 0086-29-83858046, E-mail: liyongcheng@xust.edu.cn

Copyright © 2021, Northwest Institute for Nonferrous Metal Research. Published by Science Press. All rights reserved.

layers along [010] direction.

The calculations were conducted using the Vienna Ab-initio simulation package (VASP)^[18-22] based on DFT with PAW pseudo potential method^[23]. To treat electron exchange and correlation, the Perdew-Burke-Ernzerhof formulation^[24] of GGA yielding to the correct ground state structure of Fe crystal was chosen. The cutoff energy for the plane-waves was set as 300 eV, and the supercell was large enough to ensure that the vacuum space was at least 1 nm to separate the interaction between periodic images. The atoms were relaxed using a simple conjugate gradient technique until the forces acting on each atom were smaller than 0.2 eV/nm. Brillouin zone integration was performed using the gamma-centered Monkhorst-Pack method^[25] with (1×1×7), (1×1×8), (1×1×8), (2×1×10), (2×1×10), and (2×1×12) k-points for Fe nanobelts with cross-section of 3×5, 3×7, 3×9, 3×11, 3×13, and 3×15 atom layers, respectively. To avoid the numerical instability caused by level crossing and quasi-degeneracy near the Fermi level, the Gaussian broadening method with a width of 0.1 eV was used. The optimized lattice parameter for bulk Fe was determined as 0.286 60 nm, which is in good agreement with the experiment value of 0.286 64 nm. These theoretical parameters were used in the calculations.

2 Results and Discussion

2.1 Relaxation

Since the nanobelt length along [001] direction is assumed to be infinite, there is no movement along this direction. The atoms located on adjacent (001) layer A (red square) and (001) layer B (blue circle) are shown in the same plane for convenience, and their positions before (hollow square/circle) and after (solid square/circle) relaxation for Fe nanobelts with cross-sections of 3×5, 3×7, 3×9, 3×11, 3×13, and 3×15 atom layers are presented in Fig. 2 as well. Firstly, only the representative atoms A_i and B_i within the rectangle in dashed line should be considered, because the relaxed structures retain the two-fold symmetry. Secondly, the cross-section shape changes from the rectangle into a single ellipse for the narrower Fe nanobelts with cross-sections of 3×5 and 3×7 atom layers, and then into a double-elliptic shape for the other broader Fe nanobelts. The inward relaxations for atoms at the

long side center of the broader nanobelts can be firstly observed. The inward relaxations for corner atoms and outward relaxations for atoms on the sides lead to a “round corner” phenomenon, which was observed and reported by Gall et al^[26] using the modified embedded atom method (MEAM) and tight-binding (TB) simulations. González et al^[27] tested the square prism close to a cylinder of 1D structure and a polyhedron close to a sphere of zero-dimension structure using the time-resolved HRTEM. For a completely cylindrical or spherical nanostructure, the further addition of symmetry in the radial direction can make the atom relaxation direction more isotropic, along only the negative direction of radial direction, which ensures the uniform contraction of these nanostructures. A single crystal cylinder (pillar) was observed by Uchic^[28] and Greer^[29,30] et al using a focused ion beam (FIB) microscope. Thirdly, extending the initial distance of the atoms away from the center of the nanobelts leads to an enlargement of the relaxation of the atoms in Fe nanobelts of all six sizes. Then, except the atoms remaining on the same line after relaxation, which are initially on the symmetrical dashed midlines, the atoms on the two horizontal side lines initially are not on the same line after relaxation, i. e., a “rumple” phenomenon can be observed. Finally, the inward relaxation displacement of the apex atoms is increased with increasing the size of nanobelts.

2.2 Electronic density of states

The density of states (DOS) analysis can provide better insights into the distribution of electrons with energy. Fig. 3 presents the local DOS (LDOS) and the projected DOS (PDOS) of s, p, and d orbits with majority spin (top-half) and minority spin (bottom-half) for all representative atoms, such as A_1 , A_2 , B_1 , and B_2 atoms of the Fe nanobelt with cross-section of 3×7 atom layer. Energy reference is related to the Fermi level, (E_F , the vertical dashed line in Fig.3). Firstly, for each representative atom, the LDOS curve nearly overlaps with the PDOS curve of d orbit, indicating that LDOS is mainly composed of the state of d orbit. This is because the valence electrons of Fe atom are $3d^74s^1$. Secondly, a similar LDOS curve is obtained for each representative atom on the same layer above E_F ; a decreasing trend below E_F can be observed for LDOS in the lower energy region for A and B

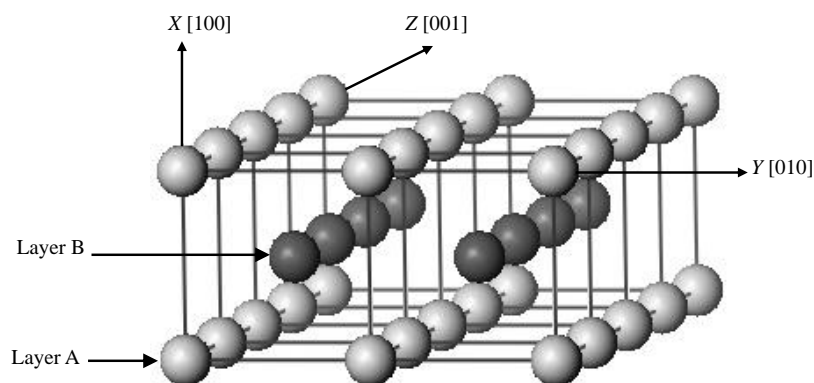


Fig.1 Schematic diagram of bcc Fe nanobelt with cross-section of 3×5 atom layer along [001] orientation

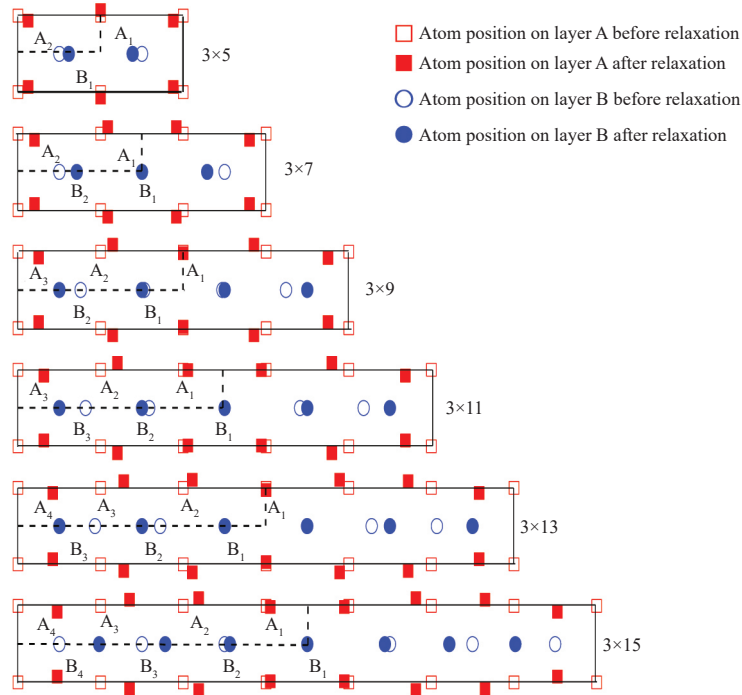


Fig.2 Atom positions on adjacent (001) layer A and (001) layer B before and after relaxation for Fe nanobelts with cross-section of 3×5 , 3×7 , 3×9 , 3×11 , 3×13 , and 3×15 atom layers (A_i and B_i represent the atoms on layer A and layer B, respectively)

layer atoms. This is attributed to the decrease in the number of the near neighbors: 2 and 4 atoms for the first nearest neighbors of A_1 atom; 4 and 5 atoms for the second nearest neighbors of A_2 atom; 8 and 3 atoms for the first nearest neighbors of the B_1 atom; 8 and 4 atoms for the second nearest neighbors of B_2 atom. Thus, it can be concluded that a smaller coordination number can lead to a decrease in LDOS in the lower energy region and an increase in LDOS in the higher energy region below Fermi level E_F .

Fig. 4 shows total DOS (TDOS) with majority spin (top-

half) and minority spin (bottom-half) for the Fe nanobelts with cross-sections of 3×5 , 3×13 , 3×7 , and 3×15 atom layers. The Fermi level is set as zero and marked by the vertical dashed lines in Fig.4. It is noted that TDOS peak is firstly increased with increasing the nanobelt size, which is clearly indicated by the fact that the blue lines in Fig.4a and 4b are both higher than the black lines. Secondly, the shapes of the curves for the Fe nanobelts with cross-sections of 3×5 and 3×13 atom layers are similar, and there is an asymmetry between the majority spin and the minority spin. Similar results can be obtained

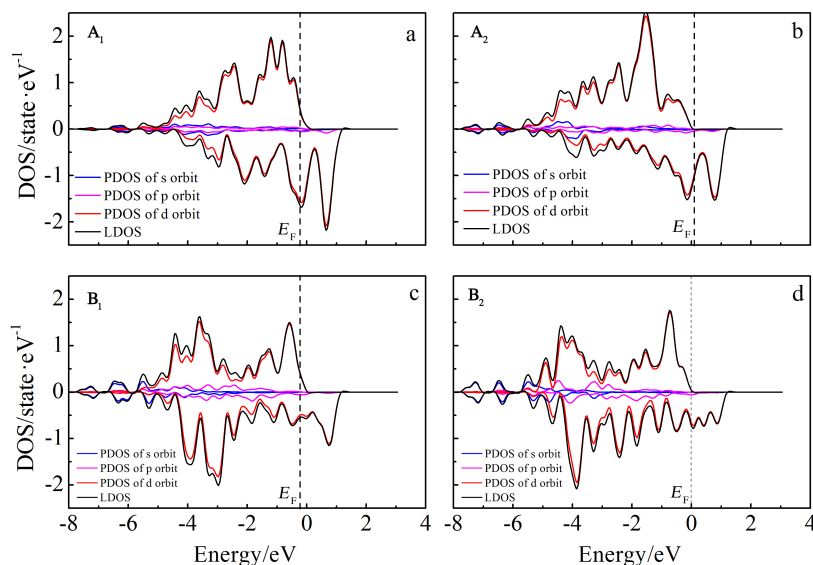


Fig.3 LDOS and PDOS s, p, and d orbitals for A_1 (a), A_2 (b), B_1 (c), and B_2 (d) atoms of Fe nanobelt with cross-section of 3×7 atom layer

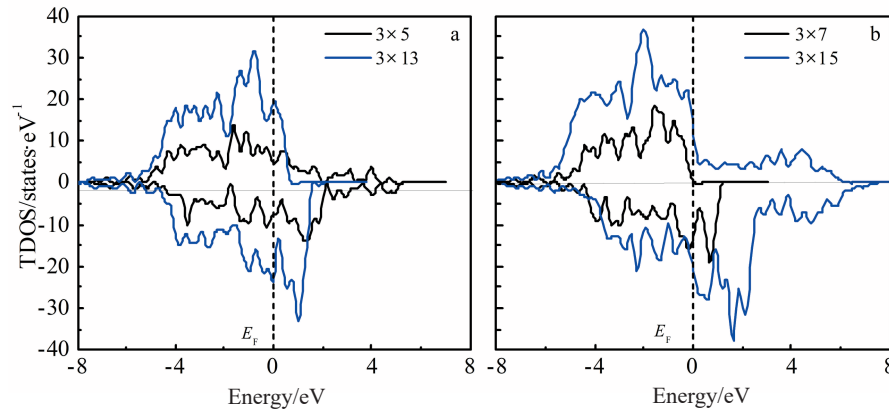


Fig.4 TDOS of Fe nanobelts with cross-sections of 3×5, 3×13 (a) and 3×7, 3×15 (b) atom layers

from Fig. 4b, indicating that these two nanobelts have high spin polarization and magnetic moment. Thirdly, TDOS in Fig.4a and 4b are slightly different, particularly at the Fermi level. This is attributed to the difference in the central atom on the center axis of the nanobelts. Fe nanobelts with cross-sections of 3×5 and 3×13 atom layers have no atom at the center, but the ones of 3×7 and 3×15 atom layers have a representative atom B_i at the center, as shown in Fig. 1. Fourthly, the Fe nanobelts with cross-section of 3×7 atom layer is found to be a half-metal material, as indicated by the fact that only one type of electrons (either majority spin or minority spin) pass through the Fermi level. These materials can be used in the field of spintronics for producing nearly

100% spin-polarized currents.

2.3 Charge density

The charge and magnetic moment projected on each representative atom A_i and B_i of Fe nanobelts with cross-sections of 3×7, 3×9, 3×11, and 3×13 atom layers are also calculated, as shown in Fig. 5. When a nanobelt is cleaved from a bulk crystal, four new surfaces are generated, and the atomic coordination numbers are reduced significantly. The neighbor atoms outside the nanobelts eventually vanish. Thus, the asymmetrical Coulomb electrostatic forces are applied to the electrons near the surfaces. In this case, the electrons must be redistributed in a three-dimensional space to ease the differences in electron density. Many surface phenomena,

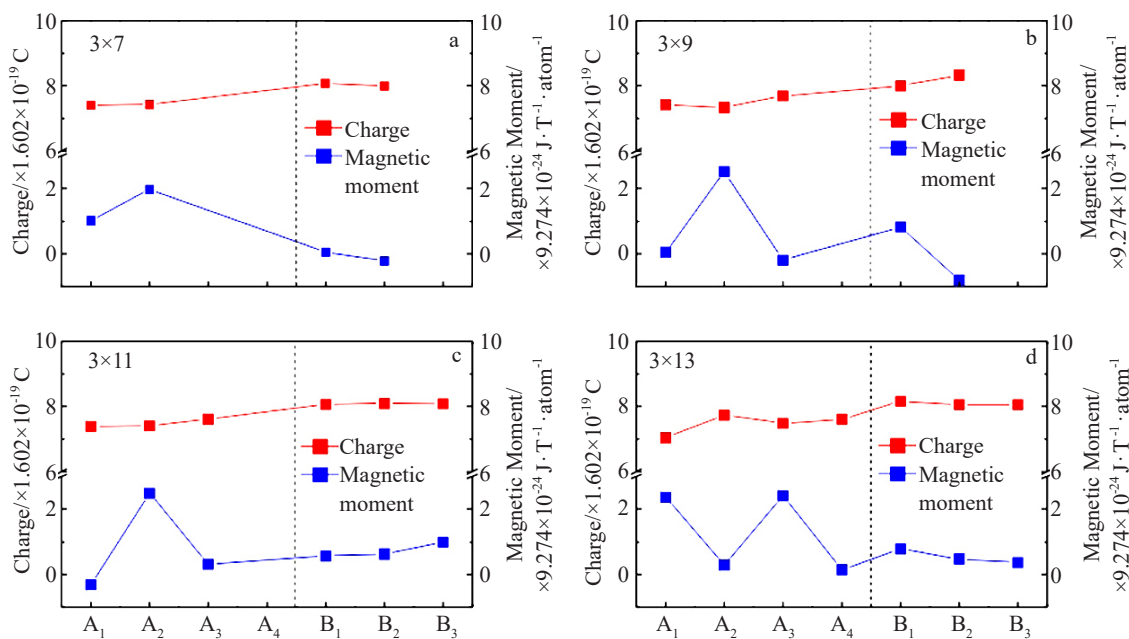


Fig.5 Total charge and magnetic moment of A_i and B_i atoms for Fe nanobelts with cross-sections of 3×7 (a), 3×9 (b), 3×11 (c), and 3×13 (d) atom layers (vertical dashed line represents the boundary of layer A and layer B)

such as surface thermionic emission, surface reconstruction, surface relaxation, surface adsorption, surface catalysis, and crystal epitaxial growth, may be related to the surface charge redistribution.

According to Fig.5, it is found that for each Fe nanobelt, the total charge shows a slowly increasing trend, but the magnetic moment shows an oscillatory phenomenon as the initial distance of the center atoms of the nanobelts decreases, especially for the representative A_i atoms. With increasing the nanobelt size, these two trends become more obvious, which also results from the decrease in the coordination numbers for atoms away from the center of nanobelt. However, such unequal decrease in coordination number, i. e., the largest, large, and small distance for vertex, edge, and center atoms, respectively, cause the redistribution of the electrons.

The bonding character of the nanobelt structures can be observed by analyzing the electronic charge density. Fig. 6 shows the charge density contours of adjacent layer A and layer B of the (001) plane for Fe nanobelts with cross-sections of 3×5 , 3×7 , 3×9 , 3×11 , 3×13 , and 3×15 atom layers, and the isodensity curves are drawn with an increment of 50

electron/nm³ from 50 electron/nm³ to 5000 electron/nm³. It can be observed that the electrons meant to share with the surface atoms vanish, because the total charge of the surface atoms is lower. It is also noted that the vanishing of the neighbor atoms outside the nanobelts leads to the fact that surface atoms start to offer their partial electrons which are meant to give to or share with the vanishing neighbor atoms to the remaining neighbor atoms. A metallic (delocalized) bonding appears obviously between the surface atoms as well as the surface atoms and their first nearest neighbor atoms, such as atom A_1 and A_1 as well as A_1 and A_2 in layer A, as shown in Fig. 6. An enhanced interaction can be observed between the vertex atoms as well as center atoms, as also reported by Da Silva et al^[31], and this phenomenon is called as metallic (delocalized) bonding character. The vanishing of the neighbor atoms outside nanobelts accompanies the vanishing of their restrictions onto the electrons of the surface atoms. As a result, most of the atoms and electrons are in the higher energy region of the occupancy state. These conclusions are applicable not only to the nanobelts but also to the nanowires, nanotubes, nanocables, clusters, and thin films. The “skin

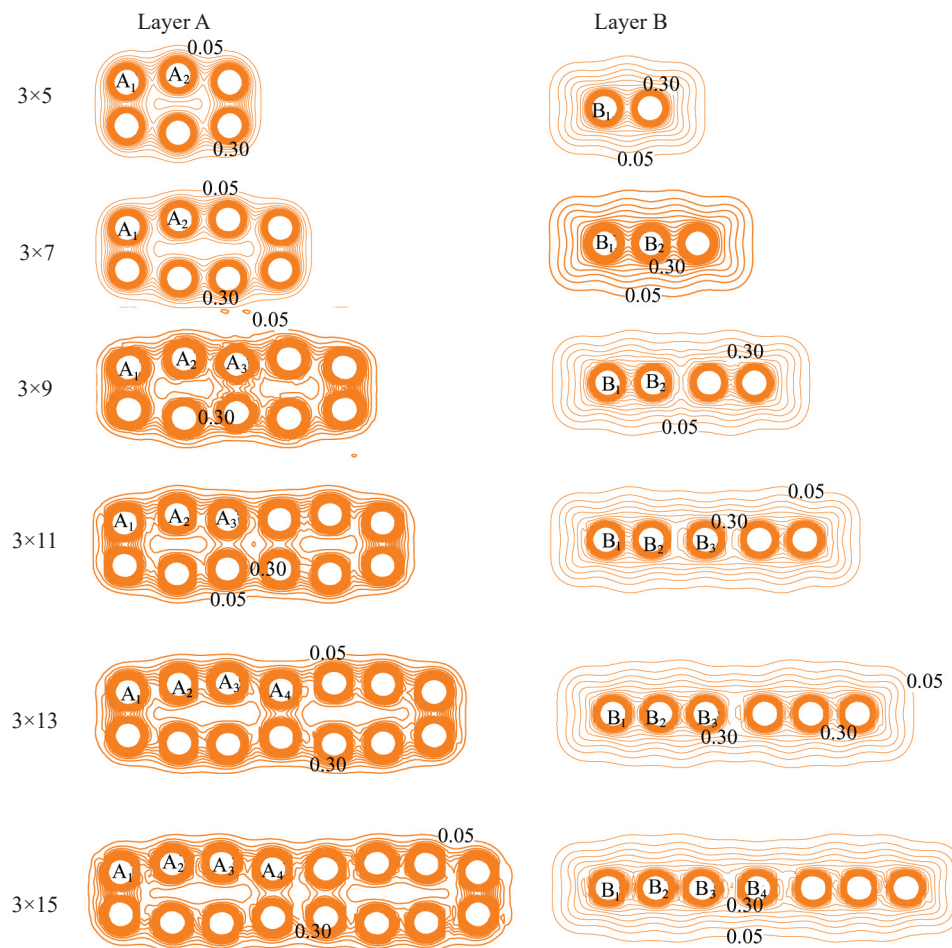


Fig.6 Charge density contours and isodensity curves of adjacent layer A and layer B of (001) plane for Fe nanobelts with cross-sections of 3×5 , 3×7 , 3×9 , 3×11 , 3×13 , and 3×15 atom layers

effect” is decreased with increasing the nanobelt size, which may be the reason why the yield strength of nanobelts and thin films is higher than that of the corresponding bulk^[32-34]. Furthermore, based on the relaxed atom structures (Fig. 2), it can be concluded that the charge density contours of the (001) plane still have the two-fold symmetry for all nanobelts in this research.

3 Conclusions

1) For Fe nanobelts with cross-sections of 3×5, 3×7, 3×9, 3×11, 3×13, and 3×15 atom layers, the relaxed atom structures retain the two-fold symmetry, but the cross-section shape changes from rectangular to elliptical, showing the “round corner” phenomenon.

2) With increasing the initial distance of the atoms away from the center of the nanobelts, the relaxation is increased.

3) The vanishing of the neighbor atoms outside the nanobelts results in two phenomena. Firstly, their electrons that are meant to share with the surface atoms vanish, because the total charge of the surface atoms is lower. Secondly, the surface atoms offer electrons which are meant to share with the vanishing neighbors to the remaining neighbor atoms, because there is an enhanced interaction between the surface atoms as well as the surface atoms and their first nearest neighbor atoms.

4) The vanishing of the neighbor atoms outside nanobelts accompanies the vanishing of their restrictions onto the electrons of the surface atoms. As a result, most of them are in the higher energy region of the occupancy state. These conclusions are applicable not only to the nanobelts but also to the nanowires, nanotubes, nanocables, clusters, and thin films.

5) Fe nanobelt with cross-section of 3×7 atom layer is found to be a half-metal material, as indicated by the fact that only one type of electrons (either majority spin or minority spin) pass through the Fermi level. Therefore, this material can be used in the field of spintronics for producing nearly 100% spin-polarized currents.

References

- 1 Song Yuzhe, Dong Jiamin, Liu Bin et al. *Rare Metal Materials and Engineering*[J], 2010, 39(4): 711 (in Chinese)
- 2 Pan A, Yang H, Liu R et al. *Journal of the American Chemical Society*[J], 2005, 127(38): 15 692
- 3 Bai X, Wang E G, Gao P et al. *Nano Letters*[J], 2003, 3(8): 1147
- 4 Hu P, Liu Y, Fu L et al. *The Journal of Physical Chemistry B*[J], 2004, 108(3): 936
- 5 Zhao M H, Wang Z L, Mao S X. *Nano Letters*[J], 2004, 4(4): 587
- 6 Bhatti H S, Gupta A, Verma N K et al. *Journal of Materials Science: Materials in Electronics*[J], 2006, 17(4): 281
- 7 Kolmakov A, Zhang Y X, Cheng G S et al. *Advanced Materials* [J], 2003, 15(12): 997
- 8 Chen Yujin, Zhu Chunling, Cao Maosheng et al. *Nanotechnology* [J], 2007, 18(28): 285 502
- 9 Bader S D. *Reviews of Modern Physics*[J], 2006, 78(1): 1
- 10 Wolf S A, Awschalom D D, Buhrman R A et al. *Science*[J], 2001, 294(5546): 1488
- 11 Zutic I, Fabian J, Sarma S D. *Reviews of Modern Physics*[J], 2004, 76(2): 323
- 12 Mangin S, Ravelosona D, Katine J A et al. *Nature Materials*[J], 2006, 5(3): 210
- 13 Li Y, Liu B G. *Physical Review Letters*[J], 2006, 96(21): 217 201
- 14 Berry C C, Curtis A S D et al. *Journal of Physics D: Applied Physics*[J], 2003, 36(13): 198
- 15 Buess M, Höllinger R, Haug T et al. *Physical Review Letters*[J], 2004, 93(7): 77 207
- 16 Bode M, Pietzsch O, Kubetzka A et al. *Physical Review Letters* [J], 2001, 86(10): 2142
- 17 Hayashi M, Thomas L, Rettner C et al. *Nature Physics*[J], 2007, 3(1): 21
- 18 Kresse G, Hafner J. *Physical Review B*[J], 1993, 47(1): 558
- 19 Kresse G, Hafner J. *Physical Review B*[J], 1994, 49(20): 14 251
- 20 Kresse G, Furthmüller J. *Computational Materials Science*[J], 1996, 6(1): 15
- 21 Kresse G, Furthmüller J. *Physical Review B*[J], 1996, 54(16): 11 169
- 22 Kohn W, Sham L. *Physical Review*[J], 1965, 140(4A): 1133
- 23 Kresse G, Joubert D. *Physical Review B*[J], 1999, 59(3): 1758
- 24 Perdew J P, Burke S, Ernzerhof M. *Physical Review B*[J], 1996, 53(7): 3865
- 25 Monkhorst H J, Pack J D. *Physical Review Letters*[J], 1976, 13(12): 5188
- 26 Gall K, Haftel M, Diao J et al. *Materials Research Society Symposia Proceedings*[J], 2005, 854: U5.7
- 27 González J C, Rodrigues V, Bettini J et al. *Physical Review Letters*[J], 2004, 93(12): 126 103
- 28 Uchic M D, Dimiduk D M, Florando J N et al. *Science*[J], 2004, 305(5686): 986
- 29 Greer J R, Oliver W C, Nix W D. *Acta Materialia*[J], 2005, 53(6): 1821
- 30 Greer J R, Nix W D. *Physical Review B*[J], 2006, 73(24): 245 410
- 31 Da Silva E Z, Novaes F D, Da Silva A J R et al. *Physical Review B*[J], 2004, 69(11): 115 411
- 32 Zhang J M, Xu K W. *Journal of Advanced Materials*[J], 2002, 34(1): 51
- 33 Kuan T S, Murakami M. *Metallurgical Transactions*[J], 1982, 13(3): 383
- 34 Li Z H, Wu G Y, Gu Y et al. *Journal of Vacuum Science & Technology A: Vacuum, Surfaces, and Films*[J], 1996, 14(5): 2693

铁纳米带半金属性的第一性原理研究

王素芳¹, 王呈岳¹, 陈立勇¹, 解 忧¹, 张建民²

(1. 西安科技大学 理学院, 陕西 西安 710054)

(2. 陕西师范大学 物理学与信息技术学院, 陕西 西安 710062)

摘 要: 基于密度泛函理论(DFT)的投影缀加平面波(PAW)赝势第一性原理, 探究了横截面为 3×5 、 3×7 、 3×9 、 3×11 、 3×13 和 3×15 原子层的铁纳米带的弛豫结构和电磁学性质。结果表明: 所有6种尺寸的Fe纳米带的弛豫结构仍具有双重对称性, 但 3×5 和 3×7 原子层的Fe纳米带的横截面形状从初始的矩形变为近椭圆形, 而其他较宽尺寸的Fe纳米带的横截面形状都变为双椭圆形。并且, 通过计算发现, 3×7 原子层的Fe纳米带是一种半金属材料, 只有自旋向上或自旋向下的电子通过费米能级, 因此可被应用于产生近100%自旋极化载流子的自旋电子学领域。

关键词: 铁纳米带; 弛豫; 电子结构; 电磁学; 密度泛函理论

作者简介: 王素芳, 女, 1983年生, 博士, 讲师, 西安科技大学理学院, 陕西 西安 710054, 电话: 029-83858046, E-mail: sufangwang@xust.edu.cn